CMS Physics Analysis Summary

Contact: cms-pag-conveners-susy@cern.ch 2012/11/20

Search for RPV supersymmetry with three or more leptons and b-tags

The CMS Collaboration

Abstract

We present a search for anomalous production of events with three or more isolated leptons produced in pp collisions at $\sqrt{s} = 8$ TeV collected by the CMS experiment at the LHC. We analyze 9.2 fb^{-1} of data collected by the CMS experiment during the 2012 LHC run. The search is applicable to any model of new physics that produces multiple leptons. We categorize observed multilepton events into exclusive search channels based on the identity and kinematics of the objects in the events and ordered by the amount of expected standard model background. We emphasize a data-based estimation of the standard model backgrounds but also use simulation to estimate some of the backgrounds when appropriate. We interpret search results in the context of *R*-parity-violating models, for which the presence of missing transverse energy is not guaranteed due to the absence of stable supersymmetric particles. We derive exclusion limits in a variety of supersymmetry topologies with *R*-parity violation and in a model that has an exotic quark.

1 Introduction

Supersymmetric (SUSY) extensions of the standard model (SM) solve the hierarchy problem and provide a mechanism for unifying particle interactions [1, 2]. Assigning R-parity as $R_\mathrm{p} = (-1)^{3B+L+2s}$, where B and L are baryon and lepton numbers, and s is the particle spin, all SM particle fields have $R_\mathrm{p} = +1$ while all superpartner fields have $R_\mathrm{p} = -1$. In models where R_p is conserved, superpartners can only be produced in pairs, and the lightest superpartner (LSP) is stable and a candidate for a dark matter particle. In addition, R_p conservation ensures proton stability. The role of R-parity in protecting the proton lifetime is an example of a more generalized "matter symmetry," which applies to theories besides SUSY wherein partner particles with differing spins are posited [3].

Models with R-parity-violating (RPV) interactions conserving either B or L in addition to s can avoid direct contradiction with the proton-lifetime upper limits [4]. The most general specification of the superpotential that is R-parity odd and renormalizable includes three trilinear R_p violating terms each parametrized by the Yukawa couplings λ_{ijk}, λ'_{ijk} or λ''_{ijk} and a bilinear term parameterized by μ_i.

$$W_{\not R_\mathrm{p}} = \mu_i H_u L_i + \frac{1}{2}\lambda_{ijk} L_i L_j \bar{E}_k + \lambda'_{ijk} L_i Q_j \bar{D}_k + \frac{1}{2}\lambda''_{ijk} \bar{U}_i \bar{D}_j \bar{D}_k,$$

where i, j, and k are generation indices, L and Q are the lepton and quark $SU(2)_L$ doublet superfields and $\bar{E}$, $\bar{D}$, and $\bar{U}$ are the charged lepton, down-like quark, and up-like quark $SU(2)_L$ singlet superfields. The fourth term violates baryon-number conservation, while the second and third terms are lepton-number violating. In this analysis, we consider R-parity-violating interactions where one of the couplings is non-zero and the rest are zero. We look for leptons in the final state coming from decays of squarks and gluinos through an intermediate particle in a variety of different topologies, allowing us to probe all three trilinear couplings.

The value of λ determines the lifetime and therefore the decay length of the intermediate particle, which in our models is the bino. Values of λ considered in this analysis correspond to decay lengths $\lessapprox 100$ μm. Our results, however, are independent of the decay length, since for low values of the decay length, the analysis sensitivity is constant. An upper limit on λ is set by constraints from neutrino-mass values. We choose values for λ that are consistent with these limits and also lead to prompt decays.

RPV interactions allow for single production of SUSY particles (sparticles) and for sparticle decay into SM particles only. The decay of the lightest SUSY particle (LSP) results in extra leptons. Due to their clean final-state multilepton signatures, processes with single-slepton production followed by decay to a pair of SM charged leptons are promising search channels for RPV SUSY particles [3]. Prior searches for RPV interactions include those by the CDF and the D0 experiments at the Tevatron [5, 6] and those by H1 [7], which have been superseded by the Compact Muon Solenoid (CMS) experiment at Large Hadron Collider (LHC) [8, 9].

The flavor content and combinations will depend on the type of coupling and the specific element of the coupling matrix that is non-zero. For example, Leptonic RPV couplings should produce four leptons, assuming all are within the analysis acceptance. If λ_{122} is non-zero, these should be all electrons and muons, but if λ_{233} is non-zero instead, then there should be two, three, or four taus with the balance being muons. We provide an summary of possible combinations of number of leptons and number of opposite-sign, same-flavor (OSSF) pairs in Table 1.

Since the LSP is unstable due to RPV, the usual experimental strategy of SUSY searches—

Table 1: Summary of possible signatures in terms of number of leptons and number of opposite-sign, same-flavor lepton pairs for different types of RPV investigated in this analysis

Coupling type	Leptonic RPV (λ_{ijk})	LQ$\bar{\text{D}}$ (λ'_{ijk})	Hadronic RPV (λ''_{ijk})
Total Number of Leptons	4	2 – 6	4
Number of OSSF pairs	0 – 2	0 – 3	2

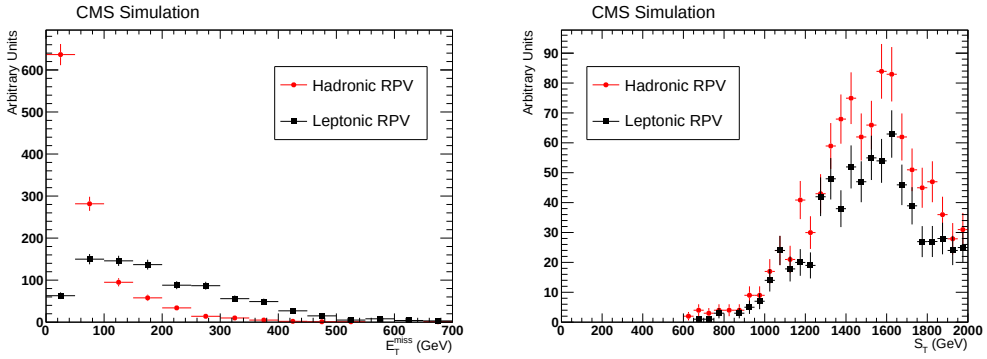

Figure 1: The $E_{\mathrm{T}}^{\mathrm{miss}}$ and S_{T} distributions for Leptonic-RPV and Hadronic-RPV models. Note that a requirement on S_{T} preserves both types of signal, while $E_{\mathrm{T}}^{\mathrm{miss}}$ does not.

selecting events with large missing transverse energy ($E_{\mathrm{T}}^{\mathrm{miss}}$)—may not be optimal [3]. We note that the Hadronic RPV events in particular fail to produce sufficient $E_{\mathrm{T}}^{\mathrm{miss}}$ in the detector, which is shown in Fig. 1. On the other hand, if the SUSY production is dominated by electroweak processes, the final state may have minimal hadronic activity. An accident of the SUSY mass hierarchy may also suppress hadronic activity despite hadronic production. For example, if the bino mass is just less than that of the squark, squark production will be effectively captured by the electroweak sector [8]. Searches that require large hadronic activity will thus be insensitive. Motivated by such considerations, we carry out a search for anomalous multilepton production in an inclusive fashion and with minimal reliance on specific kinematic properties. The search findings are then interpreted in the context of RPV models. Specifically, we search for events with three or more isolated (as defined below) final-state leptons. The data used in this analysis correspond to 9.2 fb^{-1} recorded in 2012 with the CMS detector at the LHC running at 8 TeV center-of-mass energy.

2 The CMS Detector

The CMS detector [10] has cylindrical symmetry around the pp beam axis with tracking and muon detectors within pseudorapidity $|\eta| < 2.4$. The tracking system, used to measure the trajectory and momentum of charged particles, consists of multilayered silicon pixel and strip detectors in a 3.8 Tesla solenoidal magnetic field. Particle energies are measured with concentric electromagnetic and hadronic calorimeters. Muon detectors consisting of wire chambers are at the outer radial edge of the detector. Data from pp interactions must satisfy the requirements of a two-level trigger system. The first level performs a fast selection for physics entities above a certain threshold. The second level performs a full event reconstruction.

3 Event Selection and Monte Carlo Simulation

The signal can contain electrons, muons, and the decay products from taus. In this analysis, we use electrons and muons with $p_{\mathrm{T}} \geq 10$ GeV and $|\eta| < 2.4$ which are reconstructed from measured quantities from the tracker, calorimeter, and muon system. Details of reconstruction and identification can be found in Ref. [11] for electrons and in Ref. [12] for muons.

Data for this search are collected with double-lepton triggers, as well as an electron-muon trigger. The trigger threshold is 17 GeV for the leading lepton and 8 GeV for the sub-leading lepton. To keep trigger rates manageable, there are somewhat stringent isolation requirements on the triggered electrons.

Triggers based on the scalar sum of the transverse momentum of hadronic jets H_{T} are used only for determining lepton trigger efficiencies. We use single-lepton triggers to measure the identification and isolation efficiencies of electrons and muons.

In order to ensure that the trigger efficiency is high and stable for our selected events, we require that the leading light lepton (electron or muon) in each event have a $p_T > 20$ GeV. Requiring subsequent leptons to have $p_T > 10$ GeV increases the efficiency to nearly 100% in channels with three or more leptons.

Taus can decay either leptonically (τ_ℓ) to electrons or muons, or hadronically (τ_{h}). Electrons and muons arising from τ decays are selected as described above. The hadronic decays yield either a single charged track (one-prong) or three charged tracks (three-prong) occasionally with additional electromagnetic energy from neutral pion decays. Both one- and three-prong τ_{h} decays are used in this analysis, reconstructed using the hadron plus strips (HPS) method[13].

To ensure that electrons, muons, and taus are isolated, we use the CMS particle-flow algorithm (PF) [14, 15] to identify the source of energy deposits in the trackers and calorimeters. We then sum the contribution in a cone of radius 0.3 in $\Delta R = \sqrt{\Delta\eta^2 + \Delta\phi^2}$ to calculate E_{cone}. For electrons and muons, we correct for pileup contributions and divide the summed energy by the lepton p_{T} to find the relative isolation $I_{\mathrm{rel}} = \frac{E_{\mathrm{cone}}}{p_{\mathrm{T}}}$, which is required to be less than 0.15. For hadronic taus, we require that E_{cone} is less than 2 GeV after excluding contributions originating from the wrong vertices.

We use PF-reconstructed jets [16] with $|\eta| < 2.5$ and $p_{\mathrm{T}} > 30$ GeV. Jets are required to be a distance $\Delta R > 0.30$ from any isolated electron, muon, or tau. To determine whether the jet originated from a b-quark using the combined secondary vertex algorithm, which calculates a likelihood discriminant using track impact parameter and secondary vertex information to separate heavy and light flavor jets [17].

In order to estimate the efficiencies of the lepton identification and isolation requirements, we use a tag-and-probe method [18] with $\mathrm{Z} \to \ell^+\ell^-$ events. We find that the simulation models the efficiencies correctly to within $\pm 1\%$ ($\pm 2\%$) for muons (electrons). We estimate the efficiency for isolated taus by comparing the number of $\mathrm{Z} \to \tau_\mu \tau_{\mathrm{h}}$ events in simulation to data. We use the standard recommended ratio of data to simulation for tau efficiency, which is unity with an uncertainty of 6%.

We generate Monte Carlo simulations to estimate the backgrounds of some SM processes and to understand the efficiency and acceptance of the new physics models we are investigating. The SM background samples are generated using the MADGRAPH event generator [19] and passed through a GEANT4-based [20] representation of the CMS detector. Signal samples are generated in PYTHIA [21] and passed through the light-weight detector simulation of CMS [22]. Next-to-leading order cross sections for the SUSY signal processes are calculated with Prospino [23].

4 Search Strategy

Candidate events in this search must have at least three leptons, where at most one of them is a hadronic τ. The thresholds on the transverse momenta of the leptons are chosen such that triggers used are maximally efficient on these events. The leading muon (electron) is required to have $p_T > 20$ GeV and the next to leading muon (electron) is required to have $p_T > 10$ GeV.

We classify multilepton events into search channels on the basis of the number of leptons, lepton and jet flavor, and relative charges as well as charge and flavor combinations and other kinematic quantities described below. Since the hadronic tau decays bring in additional background, search channels including these are kept separate from pure electron and muon channels.

We classify each event in terms of the maximum number of opposite-sign and same flavor (OSSF) dilepton pairs that can be made by using each lepton only once. For example, both $\mu^+\mu^-\mu^-$ and $\mu^+\mu^-e^-$ are OSSF1, $\mu^+\mu^+e^-$ is OSSF0, and $\mu^+\mu^-e^+e^-$ is OSSF2. We denote a lepton pair of different flavors as $\ell\ell'$, where ℓ indicates an electron or a muon.

Events with an OSSF lepton-pair mass below 12 GeV are rejected to exclude events with J/Ψ, Υ, low-mass Drell-Yan processes, as well as photon conversions.

We classify events as containing a leptonically-decaying Z if at least one OSSF pair has a dilepton mass ($m_{\ell^+\ell^-}$) in the Z-mass window ([75 GeV,105 GeV]). An event is considered to contain b-jets if at least one jet passes the b-tagger which uses the CMS "Combined Secondary Vertex algorithm" (CSV) [24]. The tagger has a tagging efficiency of 70% and a misidentification rate of 13% for the medium working point.

The level of SM background varies considerably across the channels. Channels with hadronic tau decays or containing OSSF pairs suffer from larger backgrounds than do channels with OSSF0. Hence all these charge combinations are considered as different channels.

For multilepton searches, the SM background is small and can be further reduced by minimal requirements on either hadronic activity or missing energy above the typical SM values. The presence of hadronic activity in an event is characterized by the variable H_{T}, defined as the scalar sum of the transverse jet energies for all jets with $E_{\mathrm{T}} > 30$ GeV. Jets used for the H_{T} determination must be well separated from any identified leptons and are required to have no isolated leptons in a cone $\Delta R < 0.3$ around the jet axis. The missing transverse energy, $E_{\mathrm{T}}^{\mathrm{miss}}$, is defined as the magnitude of the vectorial sum of the momenta of all candidate particles reconstructed with CMS's Particle Flow [16] algorithm. Comparison between data and simulation shows good modeling of $E_{\mathrm{T}}^{\mathrm{miss}}$ for processes with genuine $E_{\mathrm{T}}^{\mathrm{miss}}$ from invisible neutrinos [25, 26] and is valid for our particular selection and data collecting period as well, as will be shown later.

We define S_{T} as the scalar sum of $E_{\mathrm{T}}^{\mathrm{miss}}$, H_{T}, and the p_{T} of all isolated leptons. The S_{T} distribution peaks near the sum of the parent particle masses if most of the energy is reconstructed as leptons, jets, or $E_{\mathrm{T}}^{\mathrm{miss}}$; therefore, signal events generated by heavy particles are expected to have much larger S_{T} than SM backgrounds. The signal S_{T} distributions have very little dependence on which RPV coupling we look at. We bin the S_{T} distribution into several bins: 0-300, 300-600, 600-1000, 1000-1500, 1500-2000, 2000-2500, and above 2500. Examples of S_{T} distributions for our models are shown in Fig. 1.

5 Background Estimates

Several SM sources can produce signatures that mimic our signal. We estimate lepton fake contributions using data-driven methods, which will be described in this section. Light leptons (electrons and muons) are treated differently than taus. We estimate contributions from $t\bar{t}$, diboson, and rare process production using simulations that are validated and normalized in control regions.

5.1 Background from misidentified and non-prompt leptons

The largest background remaining after the basic three-lepton reconstruction originates from the Z+jets process (including Drell-Yan production), in which the Z boson decays leptonically and a third lepton is produced from a jet or a photon. The probability for a jet to produce an isolated lepton candidate depends on many factors, including the type of jet, the p_{T} spectrum, and the multiplicity of jets in the event. Many of these factors may be inaccurately modeled in the simulation. Therefore we estimate the background from jets with dilepton data. We relate the rate for jets to produce isolated-lepton candidates to the rate for jets to produce isolated tracks (from $K^{\pm}$ or $\pi^{\pm}$). We use events with two leptons and an isolated track to determine the number of three-lepton events where one lepton was misidentified as isolated. Similarly, we use the number of events with two leptons and two isolated tracks to determine the number of four-lepton events in which two leptons were misidentified as isolated.

The ratio of isolated-lepton rates to isolated-track rates is determined using low $E_{\mathrm{T}}^{\mathrm{miss}}$, low H_{T} data in on-Z and $t\bar{t}$ control regions, where we measure the rates in non-prompt tracks and leptons to minimize the signal contamination. The ratio of these rates is sensitive to the abundance of heavy-flavor jets in the events. To test for variation in the abundance of heavy-flavor jets we study the impact-parameter distribution of non-isolated tracks. The probability for an isolated track to fake a light lepton in dilepton data is found to be $(0.65 \pm 0.16)\%$ and $(0.6 \pm 0.15)\%$ for muons and electrons, respectively, after contributions from dileptonic decays of $t\bar{t}$ are removed. We show the relation between the ratio of the isolation efficiencies to the impact-parameter ratio in Figure 25 in the Appendix. The systematic uncertainties on these ratios come from the difference in jet properties between the QCD and dilepton samples.

For channels with τ_{h}, we extrapolate the isolation sideband $0.2 < I_{\mathrm{rel}} < 1.0$ to the signal region $I_{\mathrm{rel}} < 0.15$. The ratio of the number of τ_{h} in the two regions is $(15 \pm 3)\%$. We study the variation of this ratio for a number of QCD samples and assign a 30% systematic uncertainty for it. The ratio is applied to the dilepton event sample. We show the relation between the fake rate and jet activity in Figure. 24 in the Appendix.

5.2 Backgrounds from asymmetric photon conversions

There are two different types of photon conversions that can give rise to backgrounds in multilepton analyses. The first type is an "external conversion" into an $\ell^+\ell^-$ pair in the external magnetic field or material of the detector. This conversion is predominantly into e^+e^- pairs, and is strongly suppressed by our electron selection.

The second type of photon conversions are "internal conversions" where the photon is virtual and can produce muons almost as often as electrons. In case of asymmetric conversions, where one lepton has very low p_T and does not pass the selection criteria, Drell-Yan processes with such conversions can lead to a significant background for three lepton signatures.

We do not use the Monte Carlo approach for this background because the simulation of such asymmetric internal conversions at the matrix element level is unreliable and so is the path-

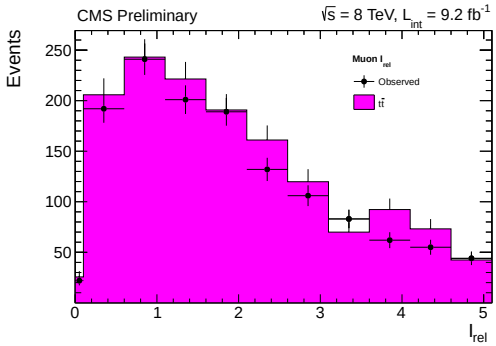

Figure 2: The isolation distribution of muons with large impact parameter ($d_{xy} > 0.02$ cm, primarily from jets) in a data sample enriched in $t\bar{t} \to \ell\nu bbjj$. The last bin contains the overflow.

tracing of the conversion pair through the detector that follows. This motivates data-based measurements of the photon to e/μ conversion factors, measured assuming the rate for the production of on-shell photons and virtual photons yielding asymmetric conversions to be proportional to each other.

We measure the conversion factors in a control region devoid of new physics (low $E_{\mathrm{T}}^{\mathrm{miss}}$ and low H_{T}). The ratio of the number of $\ell^+\ell^-\ell^\pm$ on the Z peak to the number of $\ell^+\ell^-\gamma$ on the Z peak defines the conversion factor, which is $0.35\% \pm 0.1\%$ ($1.1\% \pm 0.2\%$) for muons (electrons) [9]. The uncertainties are statistical only. We assign systematic uncertainties of 100% to these conversion factors from our underlying assumption of proportionality between virtual and on-shell photons. The measured conversion factors are then used to estimate the background in the signal regions from the observed number of $\ell^+\ell^-\gamma$ events in the signal regions. The background contribution from these converted photons is small after the final selection cuts, as will be shown in the next section.

5.3 Backgrounds from $t\bar{t}$ production

This background is estimated from simulation after careful validation in the single lepton control region enriched to be primarily $t\bar{t}$. The single lepton control region requires one isolated muon with $p_T > 30$ GeV or electron with $p_T > 70$ GeV, at least 3 jets, one of which must satisfy a high efficiency b-tag. Fig. 2 shows the relative isolation of additional non-prompt leptons in the single lepton control region in comparison with the simulation. Despite a limited number of events, good agreement between data and simulation, both in shape and normalization, is observed. We also compare the S_{T} distribution in Figure 3, which shows good agreement between the S_{T} distributions in the data and simulation.

5.4 Backgrounds from WZ production

The SM can produce 3 or more real, prompt leptons with $E_{\mathrm{T}}^{\mathrm{miss}}$ or H_{T} via diboson+jets production where both bosons decay leptonically. This class of background is referred to as "irreducible" because its characteristics are similar to the search signature. Since this background cannot be predicted directly from the data without invoking specific signal models, it must be obtained from theory and Monte Carlo simulations.

However, we correct the simulation to match measured lepton efficiencies and $E_{\mathrm{T}}^{\mathrm{miss}}$ resolution. To correct the $E_{\mathrm{T}}^{\mathrm{miss}}$ resolution, we subdivide the $E_{\mathrm{T}}^{\mathrm{miss}}$ distribution as a function the number of vertices and H_{T} in the event. A large number of vertices in an event indicates a larger extraneous energy in reconstructed objects due to pileup. This stochastic contribution results

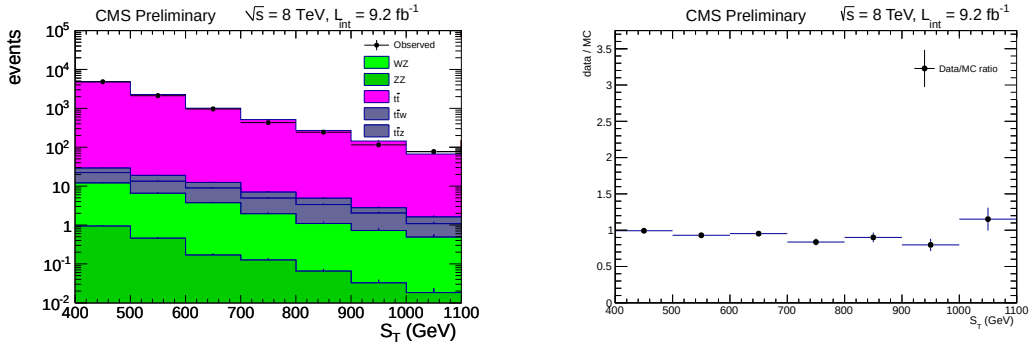

Figure 3: A comparison of data and simulation for the S_{T} distribution for events with an opposite-sign elecron-muon pair, a dataset dominated by $\mathrm{t\bar{t}}$ production shown in absolute yields (left) and as the ratio of data to simulation (right).

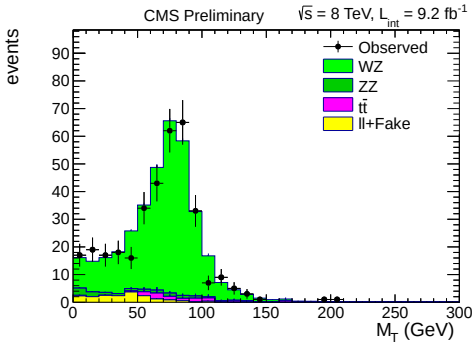

Figure 4: The transverse mass M_T distribution of events in a data sample enriched in WZ requiring an OSSF pair with $m_{\ell\ell}$ in the Z-window and $50\,\mathrm{GeV} < E_{\mathrm{T}}^{\mathrm{miss}} < 100\,\mathrm{GeV}$.

in larger $E_{\mathrm{T}}^{\mathrm{miss}}$ resolution. On the other hand, a larger H_{T} indicates higher jet activity, leading to systematically larger tails in the $E_{\mathrm{T}}^{\mathrm{miss}}$ distribution due to mis-reconstruction. We model the $E_{\mathrm{T}}^{\mathrm{miss}}$ distribution as a sum of Rayleigh distributions given by

$$p(E_{\mathrm{T}}^{\mathrm{miss}}) = \sum_{ij} W_{ij} \frac{E_{\mathrm{T}}^{\mathrm{miss}}}{\sigma_{ij}^2} e^{-E_{\mathrm{T}}^{\mathrm{miss}\,2}/2\sigma_{ij}^2}, \tag{1}$$

where "i" represents the number of vertices in the event and "j" indicates the H_T bin, and the weight W_{ij} is the fraction of events in the bin. Coefficients σ_{ij} characterize the $E_{\mathrm{T}}^{\mathrm{miss}}$ resolution in both dilepton data and the simulation. We then smear the $E_{\mathrm{T}}^{\mathrm{miss}}$ in simulation on an event by event basis to match the coefficients with data. The magnitude of the corrections varies from a few percent to as high as 30%. A 25% estimate for the systematic uncertainty of the procedure is obtained by studying the migration as a function of $E_{\mathrm{T}}^{\mathrm{miss}}$ and M_{T} as a result of an exaggerated resolution.

One can then check the simulation against control samples. We verify the simulation by comparing with data samples enriched in WZ-production, the dominant contribution to trilepton signatures from diboson+jets. WZ samples can be selected by requiring three leptons, $E_{\mathrm{T}}^{\mathrm{miss}}$, and an on-shell Z (see Fig. 4 for the tranverse mass between the lepton coming from a W and $E_{\mathrm{T}}^{\mathrm{miss}}$). We scale the WZ Monte-Carlo to match data in the region $50\ \mathrm{GeV} < M_{\mathrm{T}} < 120\ \mathrm{GeV}$.

5.5 Backgrounds from ZZ production

The ZZ sample is compared to events with four leptons including two OSSF pairs with at least one of them near the Z mass with $E_{\mathrm{T}}^{\mathrm{miss}} < 50$ GeV. We show the four-lepton invariant mass distribution for these events in data and simulation in Fig. 5.

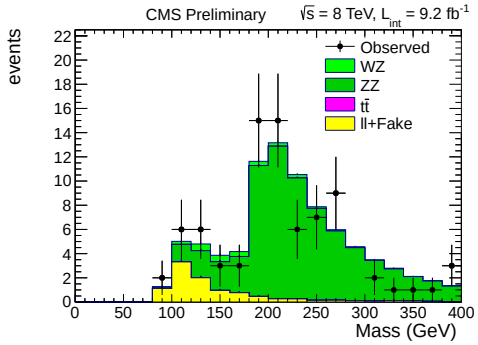

Figure 5: The four-lepton mass distribution for events with four leptons including at least one OSSF pair with $m_{\ell\ell}$ in the Z window and $E_{\mathrm{T}}^{\mathrm{miss}} < 50$ GeV.

6 Systematic Uncertainties

We assign a systematic uncertainty for the luminosity of 4.5%, which is correlated between all signal channels and the background estimates which are scaled from simulations. Uncertainties on lepton identification and trigger efficiencies discussed above also contribute to the systematic uncertainty in the result. The uncertainty on the $t\bar{t}$ background estimate contributes a large systematic uncertainty in channels where this process is prominent.

We summarize all of the systematic uncertainties in Table 2. The systematic uncertainty on the $t\bar{t}$ cross section dominates the background uncertainties for the three-lepton channels. The size of this uncertainty is governed by the limited statistics of the top-enriched control sample used to measure the isolation efficiency of μ and e from b-jets in data.

7 Results

Tables 3 and 4 show the number of observed events and the expectation from the standard model in four and three lepton events, respectively. Results for a total of 240 channels with varying levels of SM background are listed. The rows indicate the total number of isolated leptons in the event and the columns indicate the tau and b-jet content. The background estimation for all channels is performed in a uniform manner using the methods and sources described above. Figures 19, 20, 21, 22 and 23 in the Appendix show the channels as a function of S_{T} with a breakdown of the contributions to the background from different sources.

The observations and SM expectations agree within uncertainties for most channels. There are some outliers, which is to be expected with the large number of exclusive channels searched in this analysis.

We apply our search findings to RPV in models in three different topologies: a light stop RPV model, a CMSSM topology, and a squark gluino model In both topologies, we look at scenarios where the coupling λ_{ijk} for $L_i L_j \bar{E}_k$ is non-zero, examining specifically λ_{122} , λ_{123}, or λ_{233}. In the squark gluino model, we also examine the $L_i Q_j \bar{D}_k$ couplings λ'_{231} and λ'_{233}, as well as the $\bar{U}_i \bar{D}_j \bar{D}_k$ coupling λ''_{112}.

Source of Uncertainty	Uncertainty
Luminosity	4.5% [27]
PDF	14% [28]
Renormalization Scale	10% [28]
$E_{\mathrm{T}}^{\mathrm{miss}}$ Res ($E_{\mathrm{T}}^{\mathrm{miss}}$): 0-50 GeV, 50-100 GeV, $>$ 100 GeV	(-3%, +4%, +4%)
Jet Energy Scale $W^{\pm}Z$	0.5% (WZ)
B-Tag Veto (CSVM)	0.1% (WZ), 6% ($t\bar{t}$)
Muon ID/Isolation at 10 (100) GeV/c	11% (0.2%)
Electron ID/Isolation at 10 (100) GeV/c	14 % (0.6%)
$t\bar{t}$ xsec/fake rate	50%
WZ xsec	6%
ZZ xsec	12%

Table 2: We give the systematic uncertainties for several effects taken into account in this analysis. The stated values are the variation on the relevant parameters needed to cover systematic effects. Luminosity, PDF, and scale uncertainties apply to the calculated signal efficiencies only. The specific cross section uncertainties only apply to the normalization of the applicable simulated background. The remaining uncertainties apply to both signal and background efficiencies taken from simulation. The $E_{\mathrm{T}}^{\mathrm{miss}}$ resolution systematic is given for WZ background on Z for different cuts on $E_{\mathrm{T}}^{\mathrm{miss}}$ and for different cuts on M_T given a cut of $E_{\mathrm{T}}^{\mathrm{miss}} > 50$ GeV.

SUSY topologies with a light stop have received special attention since the discovery of a boson with a mass near 125 GeV[29, 30]. If this boson is the Higgs, a light stop (with mass less than 500 GeV) would be one way to keep its mass so low. However, recent searches have excluded squark and gluino masses up to between 600 and 1000 GeV[31–34]. A recent work [35] provided a comprehensive review of ways topologies with RPV could result in light stop masses that would not yet be excluded.

Using simulations provided by the authors of [35], we interpret our search in the context of models with light stop quark pair production and RPV LLE couplings λ_{122}, λ_{123}, and λ_{233}. The topology used here contains binos, sleptons, and sneutrinos with masses 100 GeV above the stop quark mass. Other particles are turned off.

Simulations for the three separate L-RPV models, four LQ$\bar{\mathrm{D}}$ models, and the one H-RPV model are generated in a grid in the squark–gluino mass plane in steps of 100 GeV, and used to calculate the signal strengths in different channels. In the Stop RPV scenario, we generate a grid for the four LLE couplings as a function of stop mass from 250 to 1500 GeV in steps of 50 GeV. Next-to-leading order, next-to-leading log cross sections are provided, in part, by the LHC cross sections group [28].

This section describes methods for setting statistical limits for various models with multiple channels. We use the LandS tool to compute limits with LHC-type CLs with 3000 toys as recommended for CMS analyses [36]. This computation yields the observed limit as well as the expected limit with one- and two-sigma uncertainty bands.

For each channel, nuisance parameters are defined to describe the systematic signal uncertainty, the systematic background uncertainty as well as the statistical uncertainties in background and signal. While systematic uncertainties in many cases are correlated across channels, statistical uncertainties are not. The datacard is produced in a way such that these correlations are taken into account properly. In order to speed up the limit computation, channels with no expected signal are removed. The channels are then ordered according to the expected single-

Table 3: Observed yields for four lepton events from 9.2 fb^{-1} recorded in 2012. The channels are broken down by the number of and mass of any opposite-sign, same-flavor pairs (whether on or off Z), whether the leptons include taus, whether there are any b-jets present and the S_T. Expected yields are the sum of simulation and data-driven estimates of backgrounds in each channel. The channels are exclusive.

			0-τ, 0-b		1-τ, 0-b		0-τ, 1 + b		1-τ, 1 + b	
N_{OSSF}	onZ	S_T(GeV)	obs	exp	obs	exp	obs	exp	obs	exp
0	-	$S_T > 2000$ GeV	0	0 ± 0.009	0	0 ± 0.009	0	0 ± 0.009	0	0 ± 0.009
0	-	$1500 < S_T < 2000$ GeV	0	0 ± 0.009	0	0 ± 0.009	0	0 ± 0.009	0	0 ± 0.009
0	-	$1000 < S_T < 1500$ GeV	0	0 ± 0.009	0	0 ± 0.009	0	0 ± 0.009	0	0 ± 0.009
0	-	$600 < S_T < 1000$ GeV	0	0 ± 0.009	0	0.01 ± 0.01	0	0.01 ± 0.02	0	0 ± 0.009
0	-	$300 < S_T < 600$ GeV	0	0.009 ± 0.01	0	0.6 ± 0.5	0	0.0007 ± 0.009	0	0.11 ± 0.07
0	-	$0 < S_T < 300$ GeV	0	0.004 ± 0.009	2	0.16 ± 0.08	0	0.0002 ± 0.009	0	0.14 ± 0.09
1	offZ	$S_T > 2000$ GeV	0	0 ± 0.009	0	0 ± 0.009	0	0 ± 0.009	0	0 ± 0.009
1	onZ	$S_T > 2000$ GeV	0	0 ± 0.009	0	0 ± 0.009	0	0 ± 0.009	0	0 ± 0.009
1	offZ	$1500 < S_T < 2000$ GeV	0	0 ± 0.009	0	0.007 ± 0.01	0	0 ± 0.009	0	0 ± 0.009
1	onZ	$1500 < S_T < 2000$ GeV	0	0 ± 0.009	0	0.01 ± 0.01	0	0.009 ± 0.01	0	0 ± 0.009
1	offZ	$1000 < S_T < 1500$ GeV	0	0.001 ± 0.009	0	0.06 ± 0.03	0	0.01 ± 0.01	0	0.001 ± 0.009
1	onZ	$1000 < S_T < 1500$ GeV	0	0.03 ± 0.02	0	0.05 ± 0.03	0	0.06 ± 0.04	0	0.02 ± 0.02
1	offZ	$600 < S_T < 1000$ GeV	0	0.02 ± 0.02	2	0.15 ± 0.05	0	0.03 ± 0.02	0	0.09 ± 0.05
1	onZ	$600 < S_T < 1000$ GeV	0	0.18 ± 0.06	0	0.7 ± 0.13	0	0.22 ± 0.13	0	0.32 ± 0.14
1	offZ	$300 < S_T < 600$ GeV	0	0.07 ± 0.02	1	0.7 ± 0.15	0	0.1 ± 0.06	0	0.47 ± 0.21
1	onZ	$300 < S_T < 600$ GeV	2	0.6 ± 0.17	5	4.7 ± 0.7	0	0.47 ± 0.25	1	0.7 ± 0.23
1	offZ	$0 < S_T < 300$ GeV	1	0.17 ± 0.05	9	4 ± 1.2	0	0.009 ± 0.01	0	0.19 ± 0.11
1	onZ	$0 < S_T < 300$ GeV	0	1.2 ± 0.38	18	18 ± 5.2	2	0.02 ± 0.02	2	0.37 ± 0.17
2	offZ	$S_T > 2000$ GeV	0	0 ± 0.009	0	0 ± 0	0	0 ± 0.009	0	0 ± 0
2	onZ	$S_T > 2000$ GeV	0	0.001 ± 0.009	0	0 ± 0	0	0.01 ± 0.01	0	0 ± 0
2	offZ	$1500 < S_T < 2000$ GeV	0	0 ± 0.009	0	0 ± 0	0	0 ± 0.009	0	0 ± 0
2	onZ	$1500 < S_T < 2000$ GeV	0	0.02 ± 0.01	0	0 ± 0	0	0.002 ± 0.009	0	0 ± 0
2	offZ	$1000 < S_T < 1500$ GeV	0	0.004 ± 0.01	0	0 ± 0	0	0 ± 0.009	0	0 ± 0
2	onZ	$1000 < S_T < 1500$ GeV	0	0.27 ± 0.06	0	0 ± 0	0	0.04 ± 0.02	0	0 ± 0
2	offZ	$600 < S_T < 1000$ GeV	0	0.04 ± 0.01	0	0 ± 0	0	0.04 ± 0.02	0	0 ± 0
2	onZ	$600 < S_T < 1000$ GeV	1	2.6 ± 0.5	0	0 ± 0	1	0.45 ± 0.14	0	0 ± 0
2	offZ	$300 < S_T < 600$ GeV	1	0.46 ± 0.1	0	0 ± 0	1	0.1 ± 0.06	0	0 ± 0
2	onZ	$300 < S_T < 600$ GeV	10	19 ± 3.8	0	0 ± 0	2	1.4 ± 0.39	0	0 ± 0
2	offZ	$0 < S_T < 300$ GeV	4	3.4 ± 0.9	0	0 ± 0	0	0.07 ± 0.03	0	0 ± 0
2	onZ	$0 < S_T < 300$ GeV	68	56 ± 13	0	0 ± 0	1	0.44 ± 0.12	0	0 ± 0
Total4	All	All	87	84 ± 19	37	29 ± 6.9	7	3.6 ± 1.1	3	2.5 ± 0.7

channel ratio of the 95% excluded cross section to the theoretical cross sections (r-value), and only the first 40 channels in this list are used to make the datacards.

When a two-dimensional parameter range is probed (such as a region in the squark–gluino mass plane), the $r = 1$ contour in the parameter plane is computed. To do so, we use interpolate between the grid points to obtain a continuous r-value landscape without gaps, in which we then determine the $r = 1$ contour with high resolution. The resulting curve is then smoothened such that misleading edges that are only due to the parameter bin size are removed.

7.1 Interpretation of the results in stop RPV

To demonstrate how natural SUSY might manifest itself with RPV couplings, we examine a stop RPV model. Fig. 6 shows the schematic of the production and decay mechanism for this simplified model.

Natural supersymmetry by definition requires stop squarks lighter than about a TeV. It is therefore worthwhile investigating signatures that arise from stop squark pair production over the full set of possibilities for stop decay modes, including through leptonic R-parity violating couplings.

The superpartner mass spectra for these benchmarks consist of a single right-handed stop squark of arbitrary mass with the bino and left and right-handed sleptons 100 GeV heavier than the stop, with the other superpartners decoupled. Production is mainly through stop squark pairs.

The leptonic R-parity violating superpotential interactions that allow the stop squark to decay

Table 4: Observed yields for three lepton events from 9.2 fb^{-1} recorded in 2012. The channels are broken down the number of and mass of any opposite-sign, same-flavor pairs (whether on or off Z), whether the leptons include taus, whether there are any b-jets present and the S_T. Expected yields are the sum of simulation and data-driven estimates of backgrounds in each channel. The channels are exclusive. The starred (*) channel was used as a control region to correct the WZ and ZZ simulations, so was not used in any interpretations.

			0-τ, 0-b		1-τ, 0-b		0-τ, 1 + b		1-τ, 1 + b	
N_{OSSF}	OSSF Mass	S_T(GeV)	obs	exp	obs	exp	obs	exp	obs	exp
0	-	$S_T > 2000$ GeV	0	0 ± 0.009	0	0 ± 0.2	0	0 ± 0.01	0	0 ± 0.2
0	-	$1500 < S_T < 2000$ GeV	0	0.01 ± 0.01	0	0.003 ± 0.2	0	0 ± 0.01	0	0.5 ± 0.48
0	-	$1000 < S_T < 1500$ GeV	0	0.07 ± 0.03	0	0.4 ± 0.22	0	0.6 ± 0.5	2	1.3 ± 0.9
0	-	$600 < S_T < 1000$ GeV	2	2.1 ± 1.2	17	9 ± 3.5	1	3.3 ± 1.6	23	20 ± 10
0	-	$300 < S_T < 600$ GeV	14	13 ± 5.7	129	134 ± 53	20	16 ± 6.5	206	186 ± 98
0	-	$0 < S_T < 300$ GeV	30	37 ± 10	555	581 ± 130	22	13 ± 5.9	150	150 ± 72
1	$m_{\ell^+\ell^-} > 105$ GeV	$S_T > 2000$ GeV	0	0.0005 ± 0.01	0	0 ± 0.2	0	0 ± 0.03	0	0 ± 0.2
1	$m_{\ell^+\ell^-} < 75$ GeV	$S_T > 2000$ GeV	0	0.002 ± 0.01	0	0 ± 0.2	0	0 ± 0.03	0	0 ± 0.2
1	onZ	$S_T > 2000$ GeV	0	0.12 ± 0.04	0	0.005 ± 0.2	0	0.01 ± 0.04	0	0 ± 0.2
1	$m_{\ell^+\ell^-} > 105$ GeV	$1500 < S_T < 2000$ GeV	0	0.08 ± 0.04	0	0.2 ± 0.2	0	0.06 ± 0.04	0	0.05 ± 0.05
1	$m_{\ell^+\ell^-} < 75$ GeV	$1500 < S_T < 2000$ GeV	1	0.02 ± 0.03	0	0 ± 0.2	0	0.06 ± 0.04	0	0 ± 0.2
1	onZ	$1500 < S_T < 2000$ GeV	2	0.5 ± 0.28	0	0.12 ± 0.08	0	0.11 ± 0.07	0	0.07 ± 0.05
1	$m_{\ell^+\ell^-} > 105$ GeV	$1000 < S_T < 1500$ GeV	0	0.46 ± 0.11	0	0.6 ± 0.28	0	0.15 ± 0.07	1	0.9 ± 0.6
1	$m_{\ell^+\ell^-} < 75$ GeV	$1000 < S_T < 1500$ GeV	0	0.41 ± 0.08	0	0.2 ± 0.12	0	0.16 ± 0.08	0	0.6 ± 0.6
1	onZ	$1000 < S_T < 1500$ GeV	6	7.6 ± 1.3	3	2.4 ± 0.5	1	1.6 ± 0.43	1	0.8 ± 0.6
1	$m_{\ell^+\ell^-} > 105$ GeV	$600 < S_T < 1000$ GeV	6	5.2 ± 1.2	12	8.5 ± 2.6	3	3.9 ± 1.5	13	9.8 ± 5.4
1	$m_{\ell^+\ell^-} < 75$ GeV	$600 < S_T < 1000$ GeV	2	4.7 ± 0.9	11	6.8 ± 2.5	0	3.3 ± 1.1	5	5.1 ± 2.8
1	onZ	$600 < S_T < 1000$ GeV	42	56 ± 7.6	48	35 ± 7.2	7	10 ± 2.7	10	6.5 ± 1.9
1	$m_{\ell^+\ell^-} > 105$ GeV	$300 < S_T < 600$ GeV	34	31 ± 5.3	149	170 ± 39	12	17 ± 6.1	80	73 ± 35
1	$m_{\ell^+\ell^-} < 75$ GeV	$300 < S_T < 600$ GeV	34	38 ± 6	139	128 ± 29	26	23 ± 9	87	81 ± 35
1	onZ	$300 < S_T < 600$ GeV	314	356 ± 45	1023	1219 ± 290	63	44 ± 8.1	131	132 ± 31
1	$m_{\ell^+\ell^-} > 105$ GeV	$0 < S_T < 300$ GeV	81	97 ± 9.5	799	761 ± 182	11	11 ± 4.6	50	41 ± 17
1	$m_{\ell^+\ell^-} < 75$ GeV	$0 < S_T < 300$ GeV	308	325 ± 36	4933	4208 ± 1033	31	35 ± 13	146	129 ± 38
1	onZ	$0 < S_T < 300$ GeV	2054*	2260 ± 213	24078	22191 ± 5517	57	67 ± 9.3	391	369 ± 87
Total3	All	All	2930	3239 ± 308	31896	29460 ± 7204	254	252 ± 59	1296	1211 ± 351

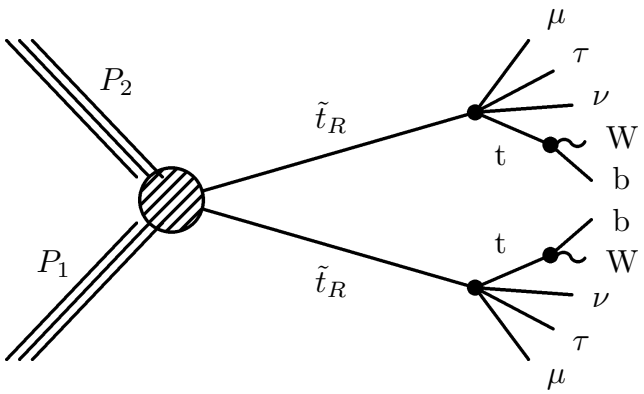

Figure 6: Diagrams of stop pair production in proton-proton collisions followed by decays leading to a final state with four leptons along with LSPs and jets in the stop RPV model. The bino and left- and right-handed slepton masses are set 100 GeV heavier than the stop quark mass, with other super partners decoupled.

are

$$W = \lambda_{ijk}\, L_i L_j \bar{e}_k \tag{2}$$

where $i, j = 1, 2, 3$ labels the flavor, and $i \neq j$. The stop decays to a top quark and intermediate off shell bino, $\widetilde{t}_R \rightarrow \widetilde{\chi}_1^{0*} + t$. The intermediate bino then decays to two leptons and a neutrino through the leptonic R-parity violating interaction, $\widetilde{\chi}_1^{0*} \rightarrow \ell_i + \nu_j + \ell_k$ and $\nu_i + \ell_j + \ell_k$. Altogether in terms of on shell particles the stop decay is four-body

$$\widetilde{t}_R \rightarrow t + \ell_i + \nu_j + \ell_k \quad \text{and} \quad t + \nu_i + \ell_j + \ell_k \tag{3}$$

The off shell particles involved in the decay are chosen to be 100 GeV above the stop mass

in order to ensure a prompt four-body decay. Starting from pair production this gives events with four leptons, two top quarks, and missing energy. Leptonic decays of the top quarks, $t \to W + b \to \ell + \nu + b$ give additional leptons. The flavor structures of the R-parity violating couplings used in three separate benchmarks are 122, 123, and 233. This gives cases with at least four leptons (electrons or muons), two tau-leptons and two leptons, and four tau-leptons. All events have two b-jets from the top quark decays.

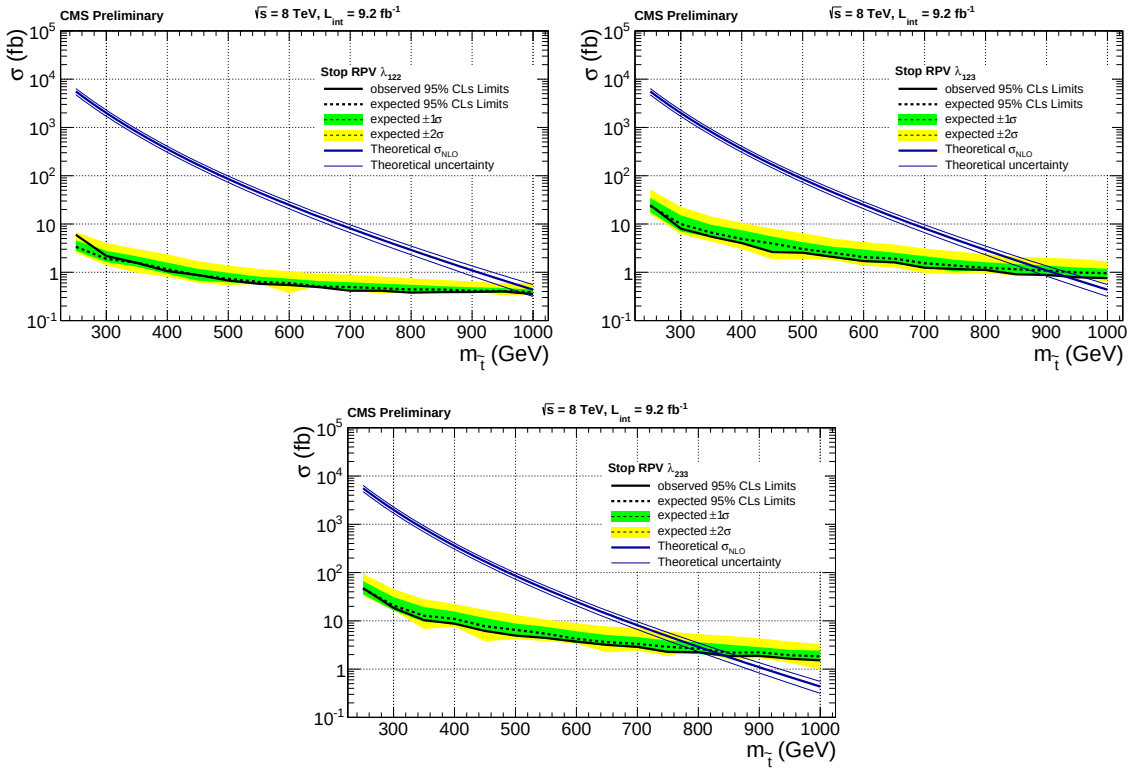

Figure 7: 95% CL limits for stop mass in models with RPV couplings λ_{122}, λ_{123}, λ_{233}.

We present the first limits on the stop mass in models with non-zero LLE couplings λ_{122}, λ_{123}, λ_{233} in Fig. 7. The acceptance improves as we approach high mass because these models produce several high p_{T} leptons, which our analysis has very high efficiency in accepting.

7.2 Interpretation of the results in Leptonic RPV

We examine Leptonic RPV as one of the characteristic models of RPV physics. Fig. 8 shows the schematic of the production and decay mechanism for this simplified model.

The superpartner mass spectra for these benchmarks are parameterized by the masses for the gluino, $\widetilde{g}$, and squarks, $\widetilde{q}$, with vanishing left-right squark mixing and flavor degeneracy. The lightest neutralino, χ_1^0, mass is fixed to be 300 GeV, and the other superpartners are decoupled. Production is mainly through pairs of squarks and gluinos, with cascade decays to the lightest neutralino and jets

$$\widetilde{g} \to \chi_1^0 + \text{jets} \qquad \widetilde{q} \to \chi_1^0 + \text{jets} \tag{4}$$

There is also a significant t-channel contribution (shown in Fig. 9). This contribution falls much more slowly as a function of gluino mass than the s-channel process.

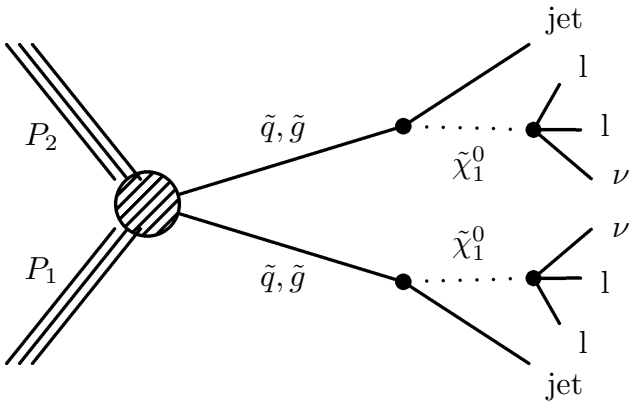

Figure 8: Diagrams of squark or gluino pair production in proton-proton collisions followed by decays leading to a final state with four leptons along with LSPs and jets in the Leptonic RPV model. The lightest neutralino has a mass of 300 GeV. Other super partners are decoupled.

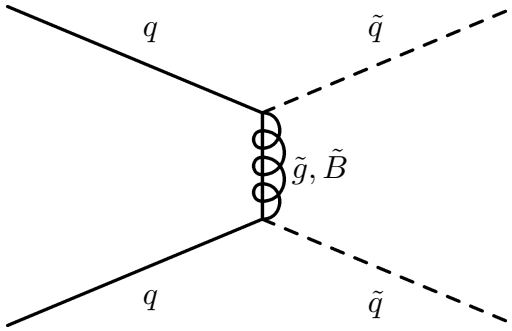

Figure 9: Feynman diagram of t-channel production process.

The lightest neutralino decays through the leptonic R-parity violating superpotential coupling

$$W = \lambda_{ijk}\, L_i L_j \bar{e}_k \tag{5}$$

where $i, j, k = 1, 2, 3$ labels the flavor, and $i \neq j$. The lightest neutralino decays to two leptons and a neutrino

$$\chi_1^0 \to \ell_i + \nu_j + \ell_k \quad \text{and} \quad \nu_i + \ell_j + \ell_k \tag{6}$$

Starting from pair production this gives events with four leptons, jets, and missing energy. The flavor structures of the R-parity violating couplings used in three separate benchmarks are 122, 123, and 233. This gives cases with four light leptons (electrons or muons), two tau-leptons and two light leptons, and four tau-leptons.

In Fig. 10, we show the 95% CL exclusion-limit contours in the parameter space of $m_{\tilde{g}}$ versus $m_{\tilde{q}}$ for models with λ_{122}, λ_{123}, and λ_{233}, along with the expected limits in the absence of observed signal. These limits substantially improve on those placed in 2011 with the 7 TeV data [9] on the same couplings.

7.3 Interpretation of the results in LQD̄ RPV

We also examine a model with a non-zero LQD̄ coupling. Fig. 11 shows the schematic of the production and decay mechanism for this simplified model.

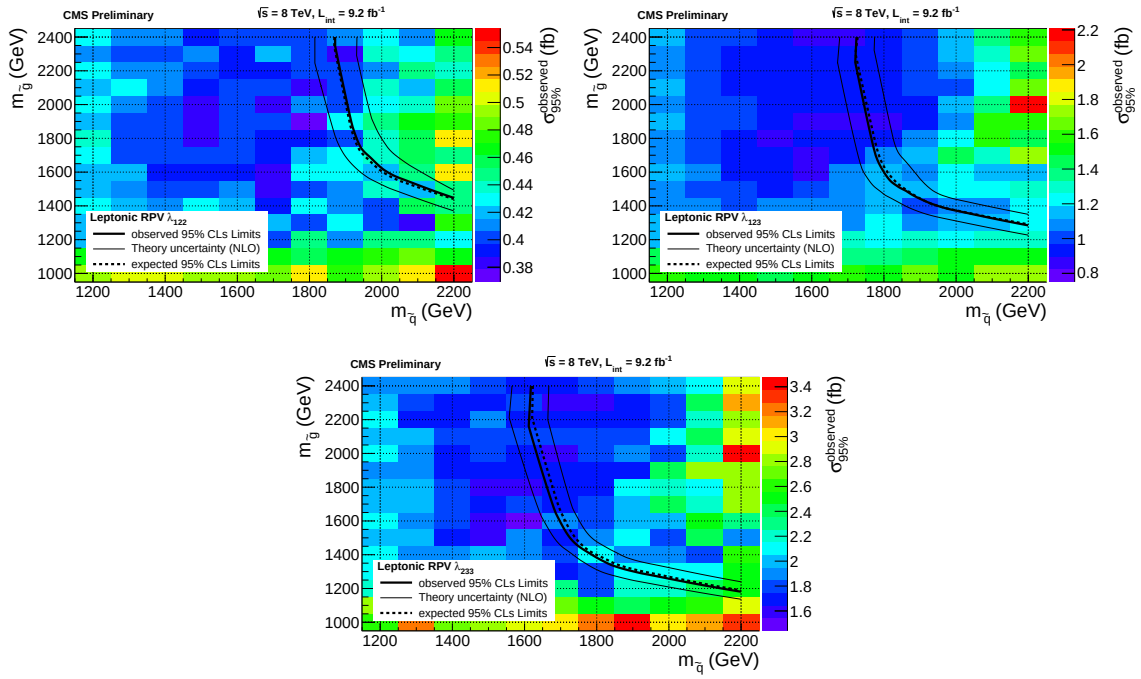

Figure 10: 95% CL limits for scenarios with Leptonic RPV couplings λ_{122}, λ_{123}, $and \lambda_{233}$ as a function of the squark and gluino masses. The observed limits, along with limits expected in the absence of signal are shown, along with the uncertainty in the expectation. Masses to the left of the curves are excluded.

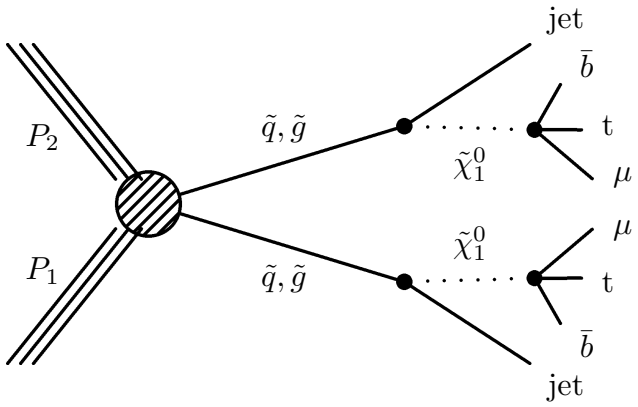

Figure 11: Diagrams of squark or gluino pair production in proton-proton collisions followed by decays leading to a final state with leptons along with LSPs and jets in the LQD̄ model. The lightest neutralino has a mass of 700 GeV. Other super partners are decoupled.

The superpartner mass spectra for these benchmarks are parameterized by the masses for the gluino, $\widetilde{g}$, and squarks, $\widetilde{q}$, with vanishing left-right squark mixing and flavor degeneracy. The lightest neutralino, χ_1^0, mass is fixed to be 700 GeV, and the other superpartners are decoupled. Production is mainly through pairs of squarks and gluinos, with cascade decays to the lightest neutralino and jets

$$\widetilde{g} \to \chi_1^0 + \text{jets} \qquad \widetilde{q} \to \chi_1^0 + \text{jets} \tag{7}$$

The lightest neutralino decays through the leptonic R-parity violating superpotential coupling

$$W = \lambda'_{ijk}\, L_i Q_j \bar{d}_k \tag{8}$$

where $i, j = 1, 2, 3$ labels the flavor.The decay modes of the lightest neutralino depend on the flavor structure of the R-parity violating coupling. The two structures used in the benchmarks are 231 and 233. For the 231 structure the decay modes of the neutralino are

$$\chi_1^0 \to \mu + t + \bar{d} \quad \text{and} \quad \nu + b + \bar{d} \tag{9}$$

For the 233 structure the decay modes are

$$\chi_1^0 \to \mu + t + \bar{b} \quad \text{and} \quad \nu + b + \bar{b} \tag{10}$$

Starting from pair production these decays give events with up to two muons and two top quarks and jets. Leptonic decays of the top quarks, $t \to W + b \to \ell + \nu + b$ give additional leptons, missing energy, and b-jets. Note that for the 231 structure all events have at least two b-jets, while for the 233 structure all events have at least four b-jets.

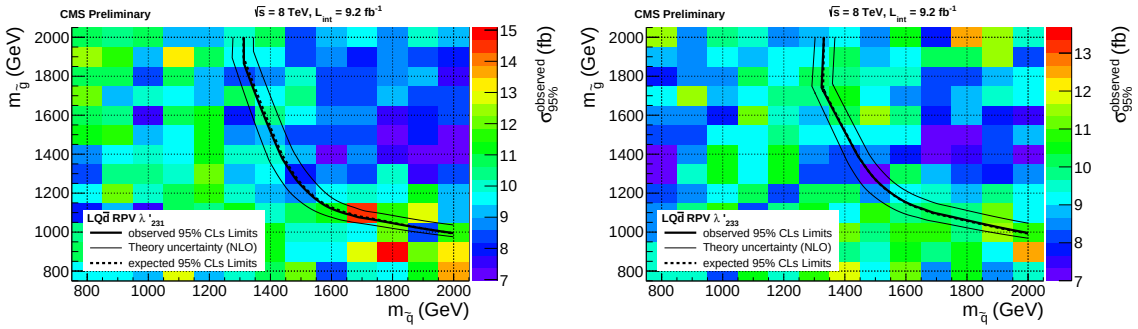

Figure 12: 95% CL limits for RPV LQD̄ couplings λ'_{231} and λ'_{233} as a function of the squark and gluino masses. The curves are shown with the observed 95% excluded cross sections.

In Fig. 12, we show the 95% CL exclusion-limit contours in the parameter space of $m_{\tilde{g}}$ versus $m_{\tilde{q}}$ for models with λ'_{231} and λ'_{233}, along with the expected limits in the absence of observed signal for the first time in the multilepton channel.

7.4 Interpretation of the results in Hadronic RPV

The Hadronic-RPV scenario provides an example of what an RPV signature might look like if there is no $E_{\mathrm{T}}^{\mathrm{miss}}$ in the final state. Fig. 13 shows the schematic of the production and decay mechanism for this simplified model.

Supersymmetric cascade decays can generically give rise to signatures with jets, leptons, and missing energy. Depending on the supersymmetric spectrum and form of the cascade decays, one or more of these main signature ingredients may be absent. This benchmark illustrates a generic class of spectra with right-handed squarks and sleptons that gives rise to jets and leptons, but with essentially no missing energy (from either stable neutralinos or neutrinos).

The superpartner mass spectra for this benchmark are parameterized by the masses for the gluino, $\widetilde{g}$, and right-handed squarks, $\widetilde{q}_R$, with vanishing left-right mixing and flavor degeneracy. A wino-like lightest neutralino and chargino, χ_1^0 and $\chi_1^{\pm}$, have fixed masses of 150 GeV, right-handed sleptons, $\widetilde{\ell}_R$, with vanishing left-right mixing have flavor degenerate masses of 300 GeV, and a bino-like second neutralino, χ_2^0, has mass a fixed mass of 500 GeV. The remaining superpartners, including the left-handed squarks, are decoupled.

Production is mainly through pairs of right-handed squarks and gluinos, with cascade decays to the bino-like neutralino and jets

$$\widetilde{g} \to \chi_2^0 + \text{jets} \qquad \widetilde{q}_R \to \chi_2^0 + \text{jets} \tag{11}$$

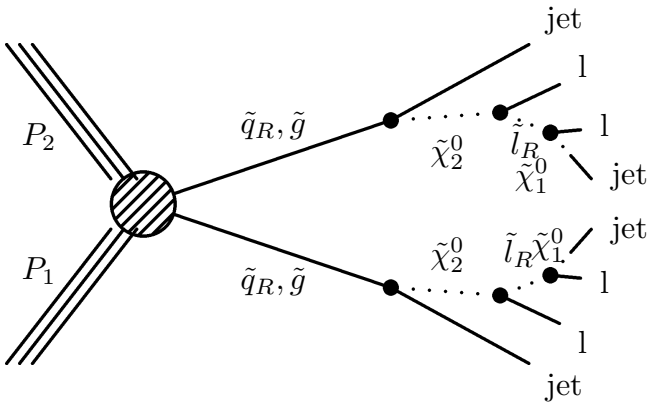

Figure 13: Diagrams of squark or gluino pair production in proton-proton collisions followed by decays leading to a final state with four leptons along with LSPs and jets in the Hadronic RPV model. This scenario has very little $E_{\mathrm{T}}^{\mathrm{miss}}$. The wino-like neutralino and charging have masses of 150 GeV. The right-handed leptons have flavor degenerate masses of 300 GeV and do not mix with the left-handed leptons. A second, bino-like neutralino has a mass of 500 GeV. The remaining super partners are decoupled.

The bino-like neutralino decays to right-handed sleptons and leptons

$$\chi_2^0 \to \widetilde{\ell}_R + \ell \tag{12}$$

The right-handed sleptons decay through bino-wino mixing to the lightest neutralino and a lepton

$$\widetilde{\ell}_R \to \chi_1^0 + \ell \tag{13}$$

Decays to the lightest chargino and neutrino are suppressed by left-right slepton mixing. The lightest neutralino decays through the hadronic R-parity violating superpotential coupling

$$W = \lambda''_{ijk}\, \bar{u}_i \bar{d}_j \bar{d}_k \tag{14}$$

where $i, j = 1, 2, 3$ labels the flavor. The flavor structure for R-parity violating coupling in this benchmark is taken to be 112. So the lightest neutralino decays through bino-wino mixing to three light flavor jets

$$\chi_1^0 \to \text{jets} \tag{15}$$

Starting from pair production these cascade decays give events with four leptons and jets, and no significant missing energy.

In Fig. 14, we show the 95% CL exclusion-limit contours in the parameter space of $m_{\tilde{\mathrm{g}}}$ versus $m_{\tilde{\mathrm{q}}}$ for a model with λ''_{112}, along with the expected limits in the absence of observed signal. These limits substantially improve on those placed in 2011 with the 7 TeV data [9] on the same coupling.

7.5 Interpretation of the results in CMSSM with RPV

In Fig. 15, we present 95% CL exclusion limit contours in the CMSSM [37] with a non-zero λ_{122} as a function of $m_{\frac{1}{2}}$, along with the expected limits and theoretical cross section for this model, which has $m_0 = 1000$ GeV, $A_0 = 0$ and $\mu > 0$.

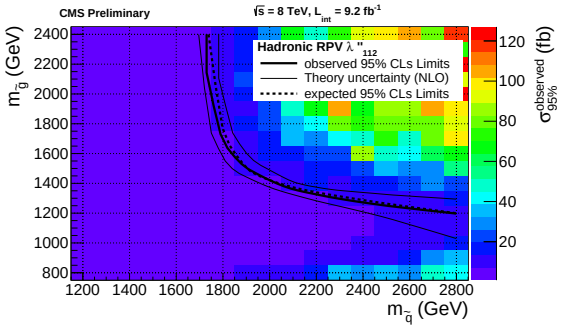

Figure 14: 95% CL limits for RPV Hadronic-RPV scenarios as a function of the squark and gluino masses. The observed limits, along with limits expected in the absence of signal are shown, along with the uncertainty in the expectation. Masses to the left of the curves are excluded. The curves are shown with the observed 95% excluded cross sections.

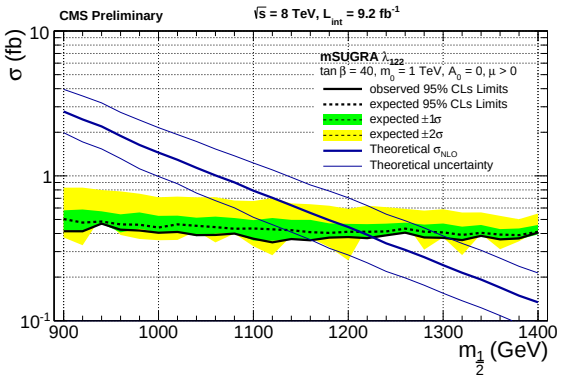

Figure 15: 95% CL limits for RPV couplings λ_{122} as a function of $m_{\frac{1}{2}}$ in CMSSM.

8 Interpretation of the result as a b'→tW or b'→bZ search

A popular idea for beyond the standard model physics is the existence of sequential, exotic quarks [38–42]. The heavier partner of the bottom quark, denoted by b', could then decay either to a top-quark with a W-boson (tW mode) or a bottom-quark and a Z-boson (bZ mode). The second mode would constitute a flavor changing neutral current (FCNC). In general, a b' would decay to both modes with non-zero branching fractions. Such an exotic quark evades bounds on a fourth generation by Higgs boson production limits. In this search, we do not consider decays of the quark to Higgs bosons.

The 7-TeV b'→bZ [43], b'→tW [44], and combined search [45] results set limits reaching 550 GeV, 611 GeV, and 685 GeV, respectively. Our multibinned approach is well-suited to search for the b' as a function of the branching fraction to the different decay modes. All the channels are treated uniformly and we present search results in a two-dimensional plane of the b' mass and the branching ratio of b'→bZ (which is 1 - BR(b'→tW) if the BR(b'→bH) is set to zero).

The various bins in the analysis have different amounts of signal as the branching ratio changes. For example, when both b' quarks decay to tW, 4.7% of events are classified as OFF-Z three-lepton events, and 0.4% of events are classified as four-lepton events. On the other hand, if both b' quarks decay to bZ, 0.36% of events have 4 leptons. When one b' decays to tW and one to bZ, then 0.375% of events are classified as 4-lepton events, and 2.25% are classified as 3-lepton events. In this way, we always have sensitivity to b' decays irrespective of the branching fractions.

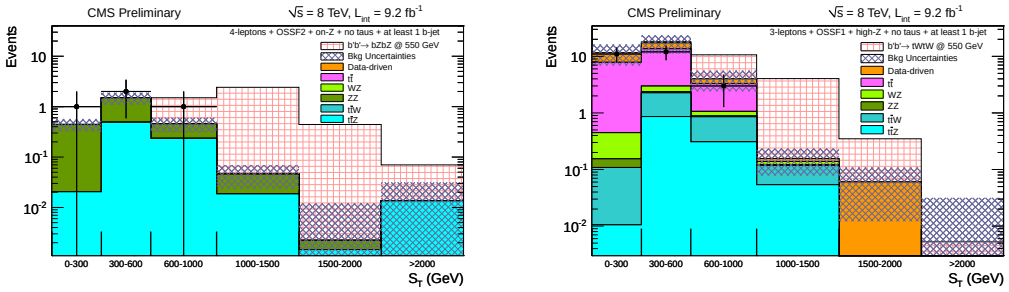

Figure 16: S_T distributions are shown for to channels with expected signals overlaid. The left plot shows the four-lepton channel with at least one b-tagged jet and one OSSF pair on the Z mass with the expected signal for b'→bZ with 100% branching ratio. The right plot shows the three-lepton channel with at least one b-tagged jet and an OSSF pair that is outside the Z window with the expected signal for b'→tW with 100% branching ratio. Both signals have a b' mass of 550 GeV.

This result represents the first CMS search for exotic quarks that presents limits as a function of branching ratio. Future work includes incorporating a third decay mode using a Higgs boson as another FCNC and adding selections and channels that improve sensitivity in the highly-boosted regime.

Figure 17 shows the exclusion as a function of the branching ratio b'→bZ on the y-axis and the b' mass on the x-axis. Points to the left of the curve are excluded at the 95% confidence level. We also show one dimensional exclusions for fixed branching ratios in Fig. 18. Cross sections are provided by the HATHOR program [46].

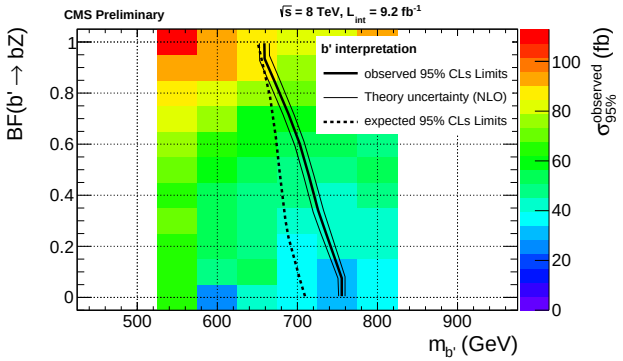

Figure 17: Exclusion in the two-dimensional plane consisting of the b′→bZ branching ratio on the y-axis and the b′ mass on the x-axis. Points to the left of the curve are excluded at the 95% confidence level.The curves are shown with the observed 95% excluded cross sections.

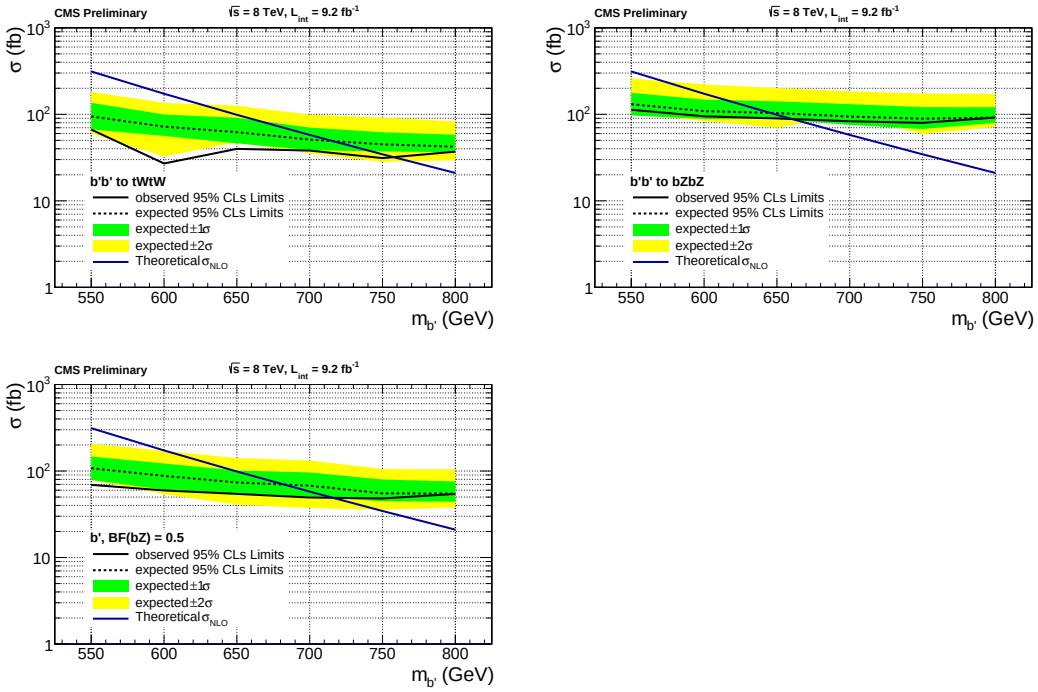

Figure 18: We show the one-dimensional exclusion contours for fixed values of the b′ branching ratio. The top left panel shows b′→tW, the top right panel shows b′→bZ, and the bottom plot shows the 50% branching ratio.

9 Conclusions

We have performed a search for RPV physics using a variety of multilepton final states. We see good agreement between observations and expectations in channels with large SM expectations both on-Z and off-Z. We have extended and improved on limits set on squark and gluino masses for models with LLE RPV couplings λ_{122}, λ_{123} and λ_{233} and HRPV coupling λ''_{112} [8, 9]. We present limits on the squark and gluino masses for models with LQ$\bar{\text{D}}$ RPV couplings λ_{231} and λ_{233} for the first time. We also show the first limits on the stop mass for models with LLE RPV couplings λ_{122}, λ_{123} and λ_{233}.

References

[1] H. P. Nilles, "Supersymmetry, Supergravity and Particle Physics", *Phys. Rept.* **110** (1984) 1, doi:10.1016/0370-1573(84)90008-5.

[2] H. E. Haber and G. L. Kane, "The Search for Supersymmetry: Probing Physics Beyond the Standard Model", *Phys. Rept.* **117** (1985) 75, doi:10.1016/0370-1573(85)90051-1.

[3] R. Barbier et al., "R-parity violating supersymmetry", *Phys. Rept.* **420** (2005) 1–202, doi:10.1016/j.physrep.2005.08.006, arXiv:hep-ph/0406039.

[4] Particle Data Group Collaboration, "Review of particle physics", *J. Phys.* **G37** (2010) 075021, doi:10.1088/0954-3899/37/7A/075021.

[5] D0 Collaboration, "Search for R-parity violating supersymmetry via the $LL\overline{E}$ couplings λ_{121}, λ_{122} or λ_{133} in $p\bar{p}$ collisions at $\sqrt{s}$ = 1.96-TeV", *Phys. Lett.* **B638** (2006) 441, doi:10.1016/j.physletb.2006.05.077.

[6] CDF Collaboration, "Search for anomalous production of multilepton events in $p\bar{p}$ collisions at $\sqrt{s}$ = 1.96-TeV", *Phys. Rev. Lett.* **98** (2007) 131804, doi:10.1103/PhysRevLett.98.131804.

[7] H1 Collaboration, "A search for squarks of Rp-violating SUSY at HERA", *Zeitschrift für Physik C Particles and Fields* **71** (1996) doi:10.1007/BF02906978.

[8] CMS Collaboration, "Search for Physics Beyond the Standard Model Using Multilepton Signatures in pp Collisions at sqrt(s)=7 TeV", arXiv:1106.0933.

[9] CMS Collaboration, "Search for anomalous production of multilepton events in pp collisions at sqrt(s)=7 TeV", *JHEP* **1206** (2012) 169, doi:10.1007/JHEP06(2012)169, arXiv:1204.5341.

[10] CMS Collaboration, "The CMS experiment at the CERN LHC", *JINST* **0803** (2008) S08004, doi:10.1088/1748-0221/3/08/S08004.

[11] CMS Collaboration, "Electron reconstruction and identification at $\sqrt{s}$ = 7 TeV", *CMS Physics Analysis Summary* **CMS-PAS-EGM-10-004** (2010).

[12] CMS Collaboration, "Performance of muon identification in pp collisions at $\sqrt{s}$ = 7 TeV", *CMS Physics Analysis Summary* **CMS-PAS-MUO-10-002** (2010).

[13] CMS Collaboration, "Performance of τ-lepton reconstruction and identification in CMS", *Journal of Instrumentation* **7** (2012), no. 01, P01001.

[14] CMS Collaboration, "Study of tau reconstruction algorithms using pp collisions data collected at $\sqrt{s}$ = 7 TeV", *CMS Physics Analysis Summary* **CMS-PAS-PFT-10-004** (2010).

[15] CMS Collaboration, "CMS Strategies for tau reconstruction and identification using particle-flow techniques", *CMS Physics Analysis Summary* **CMS-PAS-PFT-08-001** (2010).

[16] CMS Collaboration, "Commissioning of the Particle-Flow Reconstruction in Minimum-Bias and Jet Events from pp Collisions at 7 TeV", *CMS Physics Analysis Summary* **CMS-PAS-PFT-10-002** (2010).

[17] CMS Collaboration, "b-Jet Identification in the CMS Experiment",.

[18] CMS Collaboration, "Measurement of the Inclusive W and Z Production Cross Sections in pp Collisions at sqrt(s) = 7 TeV", arXiv:1107.4789.

[19] F. Maltoni and T. Stelzer, "MadEvent: Automatic event generation with MadGraph", *JHEP* **02** (2003) 027, doi:10.1088/1126-6708/2003/02/027.

[20] GEANT4 Collaboration, "GEANT4: A simulation toolkit", *Nucl. Instrum. Meth.* **A506** (2003) 250, doi:10.1016/S0168-9002(03)01368-8.

[21] T. Sjöstrand, S. Mrenna, and P. Skands, "A Brief Introduction to PYTHIA 8.1", *Comput. Phys. Commun.* **178** (2008) 852, doi:10.1016/j.cpc.2008.01.036.

[22] CMS Collaboration, "Fast Simulation of the CMS Detector", *CMS Conference Report* (2009).

[23] W. Beenakker, R. Hoepker, and M. Spira, "PROSPINO: A program for the Production of Supersymmetric Particles In Next-to-leading Order QCD", arXiv:hep-ph/9611232.

[24] CMS Collaboration, "Performance of the b-jet identification in CMS", *CMS Physics Analysis Summary* **CMS-PAS-BTV-11-001** (2011).

[25] CMS Collaboration, "Missing Transverse Energy Performance in Minimum-Bias and Jet Events from Proton-Proton Collisions at $\sqrt{s}$ = 7 TeV", *CMS Physics Analysis Summary* **CMS-PAS-JME-10-004** (2010).

[26] CMS Collaboration, "CMS MET Performance in Events Containing Electroweak Bosons from pp Collisions at $\sqrt{s}$ = 7 TeV", *CMS Physics Analysis Summary* **CMS-PAS-JME-10-005** (2010).

[27] CMS Collaboration, "Absolute Calibration of the Luminosity Measurement at CMS: Winter 2012 Update", *CMS Physics Analysis Summary* (2012).

[28] M. Kramer et al., "Supersymmetry production cross sections in pp collisions at $\sqrt{s}$ = 7 TeV", arXiv:1206.2892.

[29] CMS Collaboration, "Observation of a new boson at a mass of 125 GeV with the CMS experiment at the LHC", *Phys. Lett. B* **716** (2012) 30–61, doi:10.1016/j.physletb.2012.08.021, arXiv:1207.7235.

[30] ATLAS Collaboration, "Observation of a new particle in the search for the Standard Model Higgs boson with the ATLAS detector at the LHC", *Phys. Lett. B* **716** (2012) 1–29, doi:10.1016/j.physletb.2012.08.020, arXiv:1207.7214.

[31] CMS Collaboration, "Search for Supersymmetry at the LHC in Events with Jets and Missing Transverse Energy", *Phys. Rev. Lett.* **107** (2011) 221804, doi:10.1103/PhysRevLett.107.221804, arXiv:1109.2352.

[32] CMS Collaboration, "Search for supersymmetry in events with b-quark jets and missing transverse energy in pp collisions at 7 TeV", arXiv:1208.4859.

[33] CMS Collaboration, "Search for new physics in events with same-sign dileptons and b-tagged jets in pp collisions at sqrt(s) = 7 TeV", *JHEP* **1208** (2012) 110, doi:10.1007/JHEP08(2012)110, arXiv:1205.3933.

[34] CMS Collaboration, "Search for supersymmetry in hadronic final states using MT2 in pp collisions at $\sqrt{s} = 7$ TeV", arXiv:1207.1798.

[35] J. A. Evans and Y. Kats, "LHC Coverage of RPV MSSM with Light Stops", arXiv:1209.0764.

[36] M. Chen and A. Korytov, "Procedure for the LHC Higgs boson search combination in Summer 2011", Technical Report CMS-NOTE-2011-005, CERN, Geneva, (Aug, 2011).

[37] G. Bertone, D. Hooper, and J. Silk, "Particle dark matter: Evidence, candidates and constraints", *Phys. Rept.* **405** (2005) 279–390, doi:10.1016/j.physrep.2004.08.031, arXiv:hep-ph/0404175.

[38] P.H. Frampton, P. Hung, and M. Sher, "Quarks and leptons beyond the third generation", *Phys. Rep.* **330** (2000) doi:10.1016/S0370-1573(99)00095-2.

[39] S. Gopalakrishna, T. Mandal, S. Mitra et al., "LHC Signatures of a Vector-like b'", *Phys. Rev. D* **D84** (2011) doi:10.1103/PhysRevD.84.055001.

[40] W.-S. Hou, "Source of CP Violation for the Baryon Asymmetry of the Universe", *Chin.J.Phys.* **47** (2009).

[41] G.D. Kribs, T. Plehn, M. Spannowsky et al., "Four generations and Higgs physics", *Phys. Rev.* **D76** (2007) doi:10.1103/PhysRevD.76.075016.

[42] M. Sher, "Fourth generation b' decays into b + Higgs bosons", *Phys. Rev. D* **61** (2000) 057303, doi:10.1103/PhysRevD.61.057303, arXiv:hep-ph/9908238.

[43] CMS Collaboration, "Search B' to bZ", *CMS Physics Analysis Summary* **CMS-PAS-EXO-11-066** (2012).

[44] CMS Collaboration, "Search for heavy bottom-like quarks in 4.9 fb^{-1} of pp collisions at $\sqrt{s}$=7 TeV", *JHEP* **05** (2012) doi:10.1007/JHEP05(2012)123.

[45] CMS Collaboration Collaboration, "Combined search for the quarks of a sequential fourth generation", arXiv:1209.1062.

[46] M. Aliev et al., "HATHOR: HAdronic Top and Heavy quarks crOss section calculatoR", *Comput. Phys. Commun.* **182** (2011) 1034–1046, doi:10.1016/j.cpc.2010.12.040, arXiv:1007.1327.

A Additional Figures

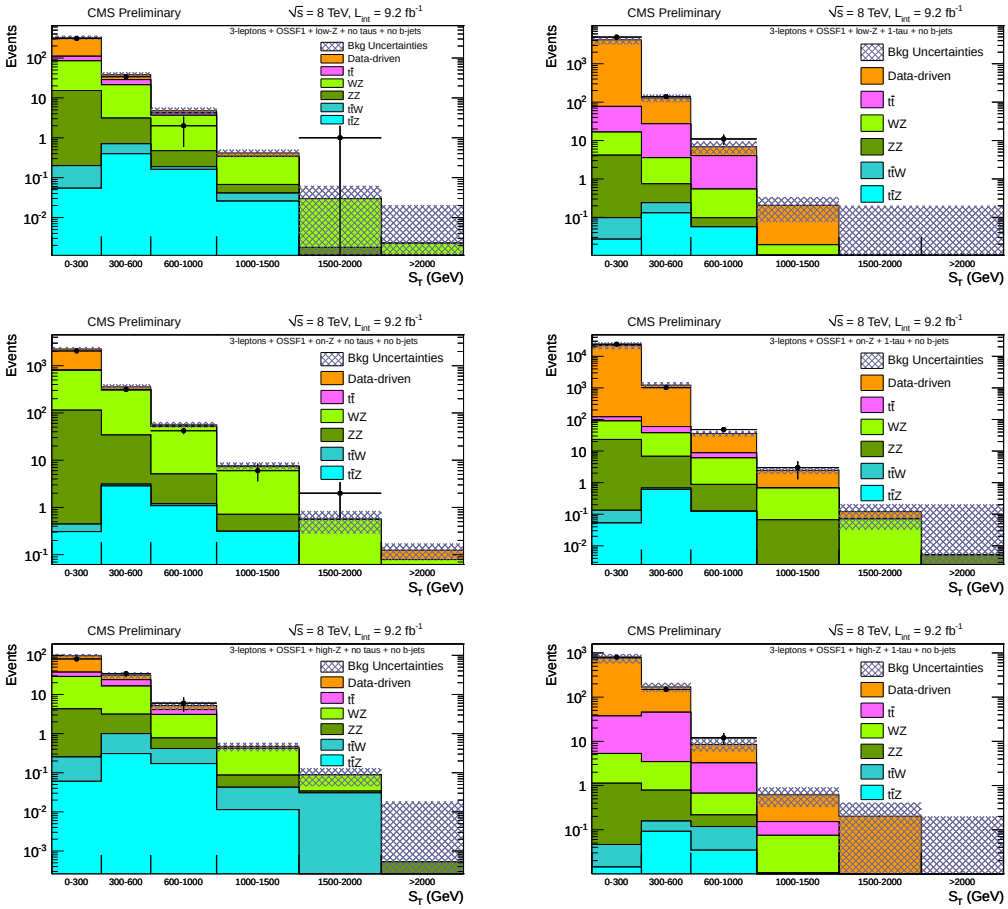

Figure 19: S_{T} distributions for three lepton channels without b-jets including an OSSF pair with $m_{\ell\ell}$ below 75 GeV (top), between 75 and 105 GeV (middle), and above 105 GeV (bottom). The left panels have zero τ_{h} and the right panels have one.

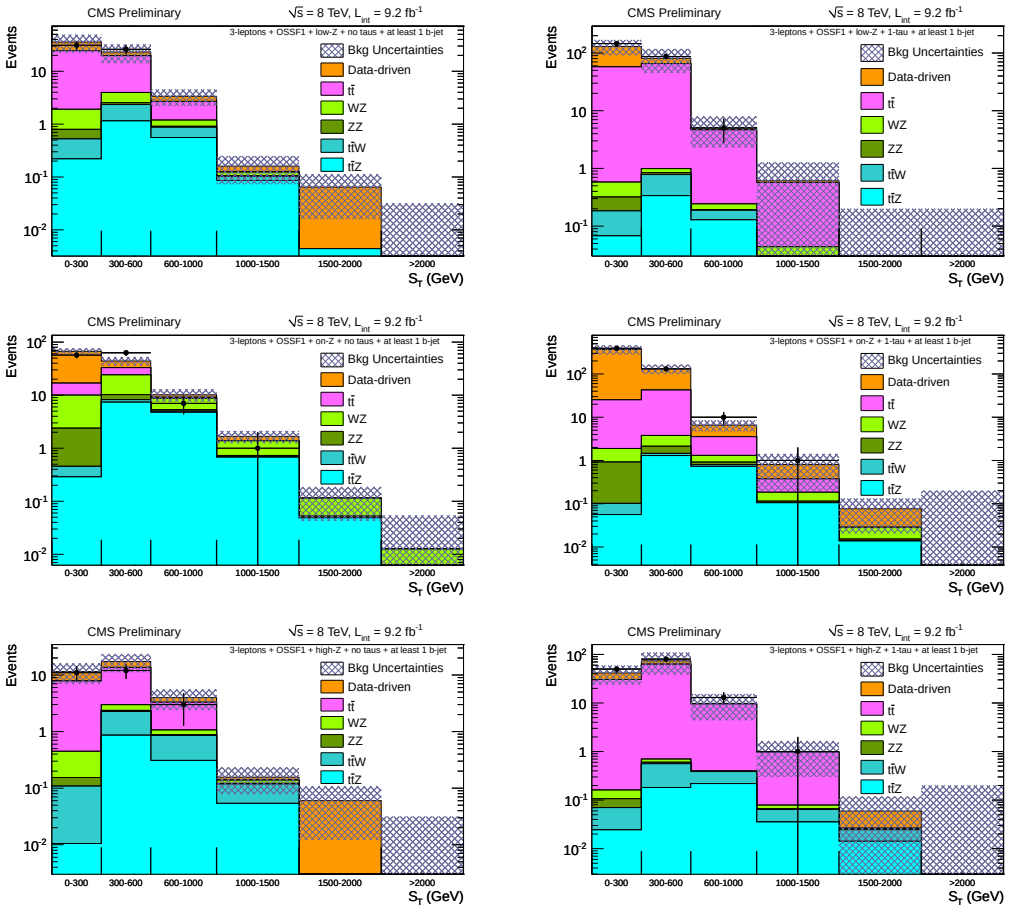

Figure 20: S_{T} distributions for three lepton channels with one or more b-jets including an OSSF pair with $m_{\ell\ell}$ below 75 GeV (top), between 75 and 105 GeV (middle), and above 105 GeV (bottom). The left panels have zero τ_{h} and the right panels have one.

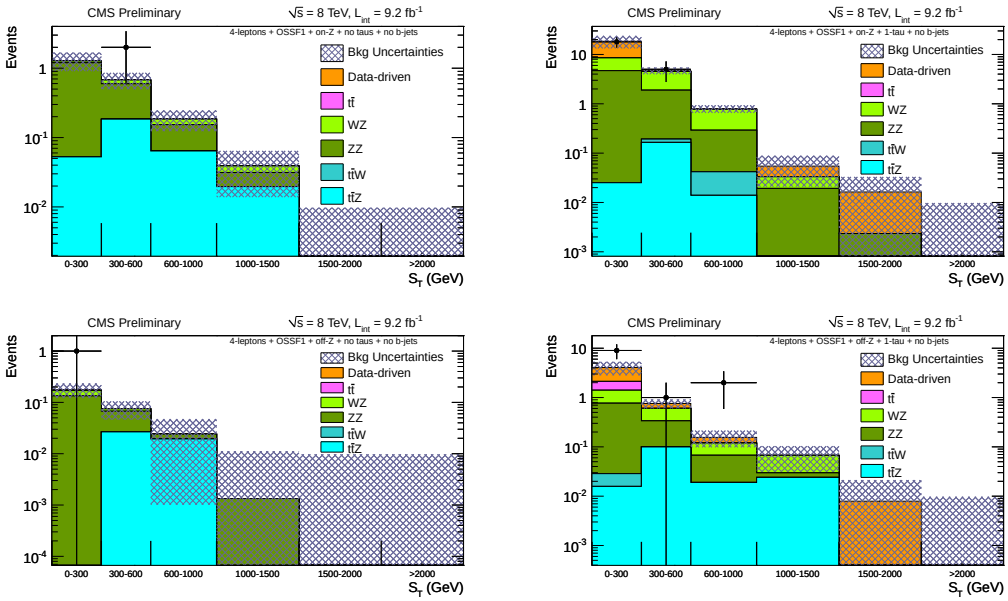

Figure 21: S_T distributions for four lepton channels with no b-jets including one OSSF pair. In the top plots, the corresponding dilepton mass is between 75 and 105 GeV, and in the bottom plots, outside that window. The left panels have zero τ_h and the right panels have one.

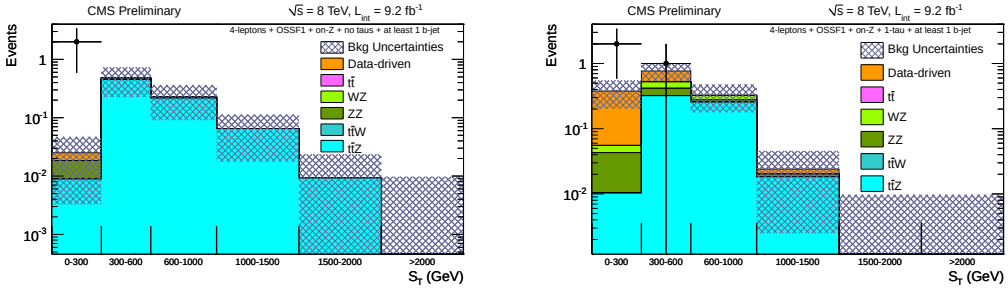

Figure 22: S_T distributions for four lepton channels with one or more b-jets including one OSSF pair where corresponding dilepton mass is between 75 and 105 GeV. The left panel has zero τ_h and the right panel has one.

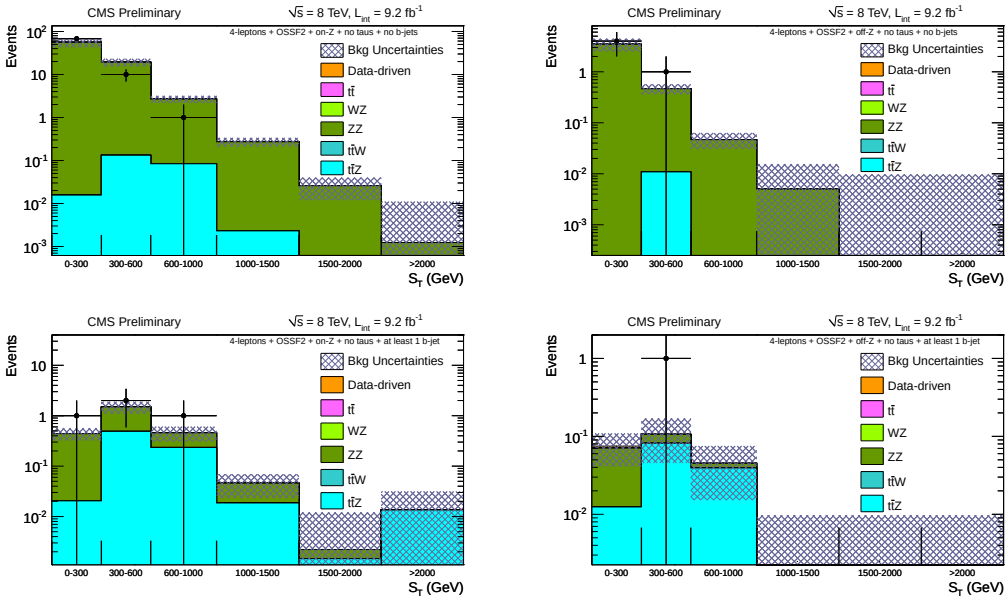

Figure 23: S_{T} distributions for four lepton channels with two OSSF pairs. In the top plots, the events are accompanied by no b-jets; on the bottom, by one or more. In the left plots, at least one of the dilepton masses falls between 75 and 105 GeV, and neither do in the right plots.

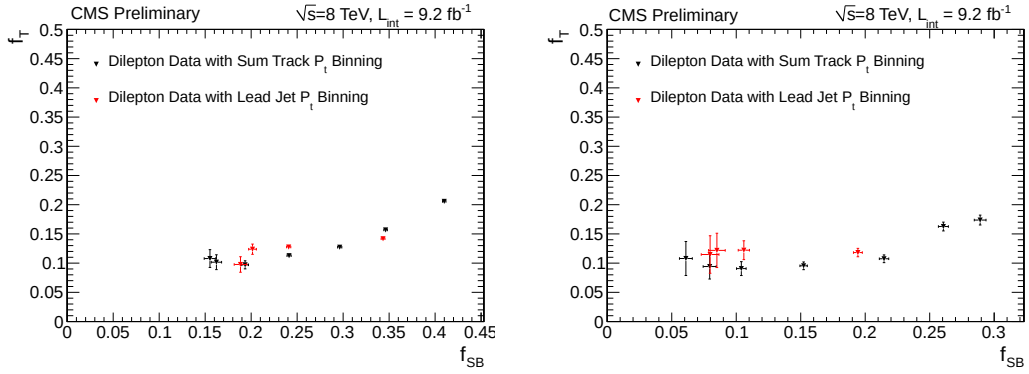

Figure 24: f_t vs f_{SB} for HPS Taus with Visible P_t between 20–40 GeV (left) and 40–60 GeV (right)

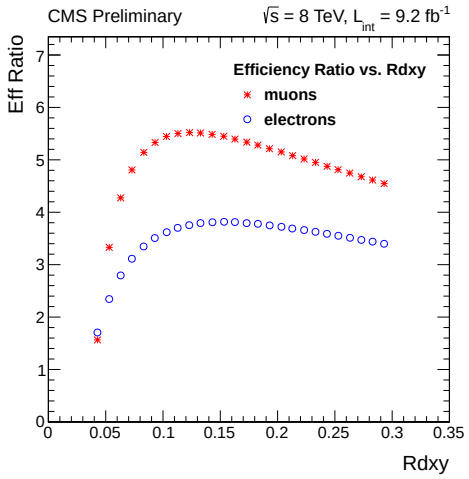

Figure 25: Efficiency ratio of leptons to tracks versus fraction of non-isolated tracks with a large impact parameter. The efficiency ratio for muons is in red and for electrons is in blue.